Journal of Thermal Science Vol.31, No.1 (2022) 25–34

**https://doi.org/10.1007/s11630-022-1553-5** **Article ID: 1003-2169(2022)01-0025-10**

# Effects of Various Geometric Features on the Performance of a 7:1 Pressure Ratio Deeply Scalloped and Split Radial Turbine in a Gas Turbine Engine

**GAO Chuang[1,2*], HUANG Weiguang[1,2]**

1. Shanghai Advanced Research Institute, Chinese Academy of Sciences, Shanghai 201210, China
2. University of Chinese Academy of Sciences, Beijing 100049, China



**Abstract:** A 2 MW gas turbine engine has been developed for the distributed power market. This engine features a 7:1 pressure ratio radial inflow turbine. In this paper, influences of various geometry features are investigated including turbine tip and backface clearances. In addition to the clearances, the effects of the inducer deep scallop and exducer rounded trailing edge are investigated. Finally, geometric features associated with a split rotor (separate inducer and exducer) are studied. These geometry features are investigated numerically using CFD. Part of the numerical results is also compared to experimental data acquired during engine test to validate the CFD results.

Results indicated that for this specific turbine, the influences of the exducer radial tip clearance, inducer axial tip clearance, and even scalloped blade backface clearance all have negligible influences on performance. In all cases, 1% increase in clearance only attributes to approximately a 0.1% lower efficiency. This finding is very different from former published papers with low pressure ratio turbines, indicating different flow physics apply for a turbine with a relatively high-pressure ratio.

**Keywords: radial turbine, high pressure ratio, scallop, leakage, clearance**

## 1. Introduction

Small gas turbines are widely used in the field of distributed energy and mobile power stations, for base or backup purposes, having the advantage of small footprint, quick response, and low emissions. For small gas turbine in the range of 0.25–2.5 kg/s air flow class, the typical configuration is a single-stage radial compressor mounted back-to-back to a single-stage radial inflow turbine [1]. At larger air flows, two stage axial turbines are favored, but there are still some exceptions mainly because of the following reasons [2]: (1) higher turbine efficiency potential due to lower tip clearance losses and reduced sensitivity to trailing edge thickness; (2) elimination of a hot end bearing in favor of the cold end/overhung rotor arrangement; (3) lower cost due to fewer parts; and (4) higher temperature capability when uncooled due to the use of higher tip speed. Examples of such large radial turbine engines include the Helan Turbines ZK2000 (2 MW), the OPRA Turbines OP16 (1.8 MW), and the Dresser-Rand KG2-3G (2 MW). The ZK2000-1A, shown in Fig. 1, features the highest-pressure ratio (PR=7.5) and an annular combustor while the other two utilize cannular combustor.

For these engines, the radial turbines are unusually large. Taking the one used in ZK2000 as an example, the inducer outer diameter is approximately 550 mm while

Article type: Contributed by Asian Congress on Gas Turbines 2020 (August 18–19, 2021, China).
Received: Oct 15, 2021 Corresponding author: GAO Chuang E-mail: gaoc@sari.ac.cn

**Nomenclature**

| | | | |
|---|---|---|---|
| $b$ | backface gap height | $s_1$ | span, blade height at leading |
| $C_p$ | static pressure coefficient | $s_2$ | span, blade height at trailing |
| $d_1$ | shroud axial movement distance | $t$ | tip gap height |
| $d_2$ | shroud radial movement distance | $V$ | velocity |
| $d_3$ | hub axial movement distance | **Greek symbols** | |
| OPR | output power ratio | $\eta_{ien}$ | isentropic efficiency (total to total at rotor exit) |
| $m$ | mass flow | $\theta_s$ | shroud rotating degree |
| $\dot{m}$ | mass flow rate | $\theta_h$ | hub rotating degree |
| $p$ | static pressure | $\rho$ | density |
| RL | radial location | **Subscripts** | |
| $S_m$ | meridional length | 3 | rotor inlet |

the tip speed is nearly 700 m/s, which exceeds nearly all existing production radial turbines. In these large tip speed turbine designs, to reduce weight and centrifugal stress, a deep scallop between inducer blades is always used. As shown in Fig. 2, with the deep scallop, radial turbine does not extend out to the blade tip which incurs both the tip clearance and the backface clearance. The latter clearance is usually the largest one in radial turbine. Simonyi et al. [3] presented a comparison of a computational and test performance for three deeply scalloped radial turbines. It was found that the efficiency penalty due to the backface clearance was nearly 60% of the total clearance losses. Rodgers [1] used the net equivalent shroud which is defined as front shroud clearance plus 0.5 times the back shroud clearance for deeply scalloped turbine. He and his co-workers [4] numerically investigated the backface cavity sealing flow in deeply scalloped radial turbines. Different cavity configurations and their effects on the flow structure and turbine performance were studied both using steady and unsteady numerical methods. In addition, they [5] conducted a numerical study of flow structure and heat transfer in the backface clearance. It was found that the leakage flow is very strong in the tip region whereas the scraping flow dominates over the clearance in the lower radial region.

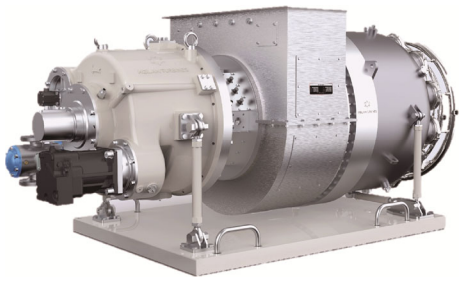

**Fig. 1** ZK2000 2 MW gas turbine engine

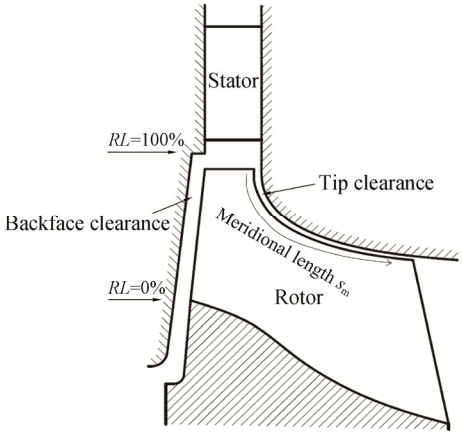


**Fig. 2** Meridional view of the turbine flow passage

In addition to turbine backface clearance, shroud tip clearance effects have been covered by many publications. Futral and Holeski [6] calculated a reduction of 0.15% in efficiency for each percent increase in axial clearance at rotor entrance. However, a 1.6-percent decrease in efficiency for each percent increase in radial clearance at the rotor exit, which is about 10 times as compared with the rotor inlet clearance effect. Dambach and co-worker [7, 8] measured the detailed velocity and pressure fields in the tip clearance of a radial turbine and recorded similar trends to those of Futral and Holeski [6]. Dambach etc. [9] led an experimental study of tip clearance flow in a radial inflow turbine. Their research showed that there is little tip leakage in the first part of the rotor because of the effect of scraping and the bulk of tip leakage flow in a radial turbine passes through the exducer which brings a higher tip gap loss. Deng etc. [10] numerically studied the effect of varying blade-shroud clearance on the leakage flow in radial inflow rotor. They found that regardless of the tip clearance transverse mass flow rate, the curves strongly exhibit the characteristics of linearity when the relative meridional length is greater than 40%. Furukawa etc. [11] studied the process of the tip leakage vortex breakdown in a compressor rotor by numerical method. They found that the leakage vortex breakdown

plays a major role in characteristic of rotor performance at near-stall conditions. They further found that measures such as a circumference slot, axial slot, or honeycomb applied and placed at the shroud surface over the exducer can reduce the transverse flow [10].

Perhaps the most common method to achieve low leakage is to utilize a covered (shrouded) impeller. Wen Li et al. [12] conducted experimental and numerical investigations of a covered radial inflow turbine with labyrinth seals. The results indicated that the labyrinth seal flow has no effect on the main flow passage with primary losses due to the seal leakage mass flow. Liu etc. [13] studied secondary flow injection, specifically the mass flow rate and direction, on the radial turbine performance. They found that injection increases the power output of the turbine. If the injection can be performed without any additional system power output, recover exhaust gas for example, the net performance improvements can be very significant. Huang etc. [14] investigated the effects of the synthetic jet control and the interaction with the tip leakage flow in centrifugal impeller at the near-stall working point using unsteady numerical analysis.

All the work documented in the previously mentioned references was performed on turbines with low pressure ratio and relatively low tip speed. One exception is the research performed and documented by Jones [2].

In this paper, analysis of the turbine used in the ZK2000-1A gas turbine engine will be presented in detail. This turbine has the highest known tip speed of existing production radial turbines. Due to the specific engine configuration, during operation, the turbine rotor tip and backface clearances vary simultaneously. This effect is the result of nozzle rotation in the *R-Z* (meridional) plane due to thermal gradients in the nozzle shroud and hub. This is also different from existing research of which the tip clearance is varied independently, either axially or radially.

Another feature of the ZK2000 turbine is the fact that the rotor fabricated in two pieces (separate inducer and exducer). This two-piece design is required due to its relatively large size, high tip speed, and small length to diameter ratio. For these reasons, the use of a single piece forging or casting is not possible. Although the two-piece turbine presents additional problems of assembly, there are some definite benefits including: (1) freedom to choose separate materials for inducer and exducer based on thermal load and stress; (2) flexibility to design the thickness and shape of inducer and exducer blades independently; (3) being able to add damping at the blade interface, which is beneficial for avoiding natural frequency excitation. The two-piece design, however, creates additional challenges in regards to aerodynamic design. There is an additional axial clearance along with a surface discontinuity between the inducer and exducer blades. An angular dislocation caused by preload during assemble is complicated by thermal and centrifugal loading during operation.

For a future application, this 2 MW gas turbine will be directly connected to a high-speed generator, and it has to have variable speed capability. That complicates the design regarding frequency analysis of the exducer blade first flap mode. To address this issue, an alternate exducer design was created featuring a significantly rounded trailing edge to increase the blade stiffness. The rounded trailing edge will greatly reduce the exducer axial length at the tip, or radial clearance. To the authors' knowledge, there is no publication discussing this specific issue.

The paper is organized as follows: 1. Introduction; 2. ZK2000 engine and turbine geometry features; 3. Numerical methods; 4. Calculated results and discussion; 5. Conclusions and acknowledgement.

## 2. Engine Background and Turbine Parameters

Analyses of two different turbines are presented in this paper. The first is for the original design gas turbine with a simple thermal cycle having a power output of 2000 kW (ZK2000S). The second is for a modified version of the engine having a recuperated thermal cycle (ZK2000R). Fig. 2 shows the meridional view of the turbine stage and Table 1 lists the design parameters for turbines of ZK2000S and ZK2000R.

**Table 1** Turbine parameters for ZK2000S and ZK2000R

| Design parameters | ZK2000S | ZK2000R |
|---|---|---|
| Vane number | 23 | 29 |
| Blade number | 13 | 13 |
| Expansion ratio | 7.2 | 7.2 |
| Turbine inlet temperature/K | 1223 | 1223 |
| Mass flow rate/kg·s$^{-1}$ | 10 | 10 |
| Rotating speed/r·min$^{-1}$ | 24 000 | 24 000 |

## 3. Numerical Methods

In order to better represent the real geometries, due to their flexibility, unstructured grids are used to discretize the simulation domain in a sector modelling approach. At least 10 layers of prisms are inserted adjacent to any wall boundaries with the most adjacent prism layer thickness being controlled to ensure that the wall $y^+$ value is less than 10. To ensure mesh independence, a grid sensitivity study was initially performed, resulting in a total number of about 3×106 grid points. Fig. 3 shows the turbine mesh of ZK2000S. Meshes for the other turbine stage are similar. The simulation work was done with the help of Helan Turbines Co., Ltd.

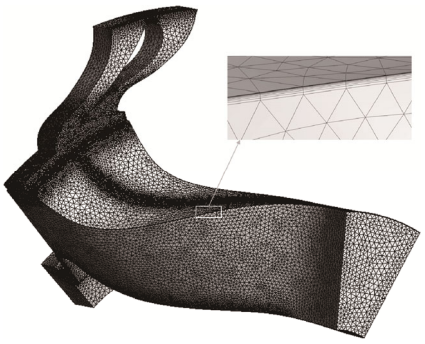

**Fig. 3** Mesh for the Turbine stage of ZK2000

The commercial code ANSYS CFX 18.0 is used to simulate the physical models, solving the Reynolds Averaged Navier-Stokes (RANS) equations closed by turbulence modelling and gas state equations. The SST turbulence model, which gives accurate prediction of flow separation, is used during the simulation. In terms of the inlet boundary, total temperature, total pressure, and turbulence properties are specified. For the outlet boundary, static pressure is specified. Rotational periodic boundary conditions are imposed on the periodic boundaries. Mixing plane GGI interfaces are used to connect the static and rotational domains. Fluid results in the rotor region are calculated under relative coordinates with the rotating speed set to be that at the design condition. Non-slip adiabatic conditions are specified at all the solid walls. A counter-rotating wall condition is specified for the backface and rotor shroud walls.

In order to validate the CFD method, experiment results are compared with CFD results. Table 2 shows the comparison of the isentropic efficiency of ZK2000S turbine between the engine test and CFD results, and good agreement can be seen. This value is an estimate based on cycle balance.

**Table 2** Comparison of the isentropic efficiency of ZK2000S between the experiment and CFD results

| | Experiment | CFD |
|---|---|---|
| $\eta_{ien}$ | 89.6% | 90.8% |

## 4. Results and Discussion

### 4.1 Effect of the tip clearance flow

Since the radial turbine is the component receiving hot gas from the combustor, it experiences deformation and rotation from the engine cold condition to hot condition, and this causes the clearances to change.

In this section, the effect of tip clearance changing due to rotation of the rotor shroud as shown in Fig. 4, is analyzed. Five cases of $\theta_s$ are calculated and compared, namely –0.5°, ori (zero rotation), 1°, 2°, and 3°. Their tip gap heights (clearance) versus meridional length $S_m$ are compared in Fig. 5. As shown in Fig. 5, the tip gap height ($t$) increases more significantly near the blade trailing than the blade leading as $\theta_s$ is increased. The isentropic efficiency, $\eta_{isen}$, and the output power ratio, OPR, against $\theta_s$ are shown in Fig. 6. OPR is the calculated turbine output power normalized by the designed engine output power, which is 2000 kW for ZK2000. As expected,

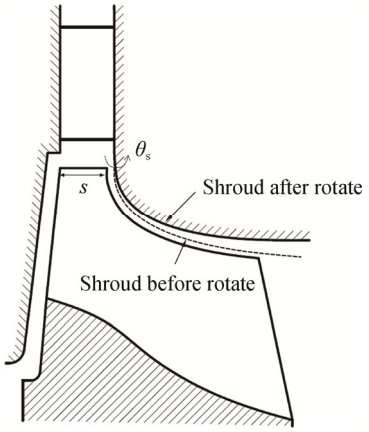


**Fig. 4** Meridional view of the tip clearance changing due to the shroud rotating

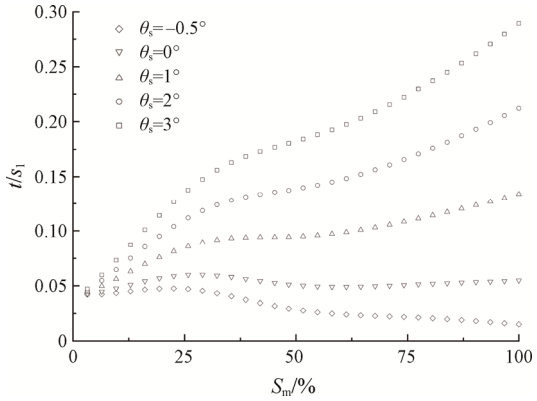


**Fig. 5** Variation of the tip clearance height against $S_m$ for different $\theta_s$ cases

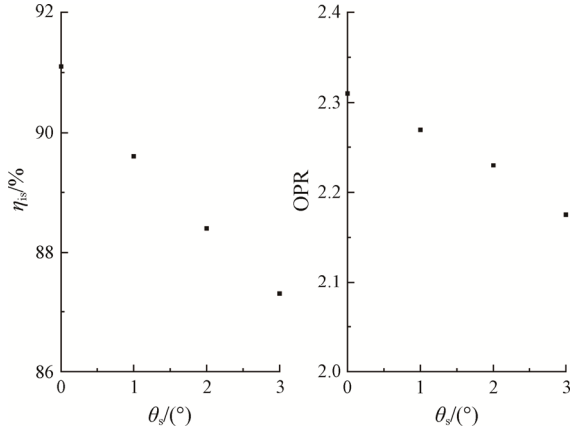


**Fig. 6** Isentropic efficiency and output power against $\theta_s$ for ZK2000S

when the rotating angle increases, the tip clearance is enlarged, hence leading to lower efficiency and output power. The reduction of the efficiency is almost linear, 1° of change of the shroud rotation resulting in approximately 1.3 percent performance reduction.

The nature of the tip clearance can also be changed when the rotor shroud moves axially, as illustrated in Fig. 7. Four cases of axial movement measured at location $d_1$ (Fig. 7), are calculated, and compared. They are 0 mm (original, no axial movement), 0.5 mm, 1 mm, and 1.5 mm. Their tip gap heights against meridional length $S_m$ are compared and shown in Fig. 8. Increasing the axial movement parameter $d_1$ mainly increases the tip clearance height before 60% meridional length, beyond which there is little change in clearance height. Fig. 9 shows the isentropic efficiency, $\eta_{isen}$, and the output power ratio, OPR (over all pressure ratio), against $d_1$ for the ZK2000S. As $d_1$ increases, a large portion of the tip clearance is enlarged, leading to a larger leakage flow and worse turbine performance. The reductions of efficiency and output power are linear, a 1% increase of shroud axial movement leading to approximately 0.15 percent efficiency reduction.

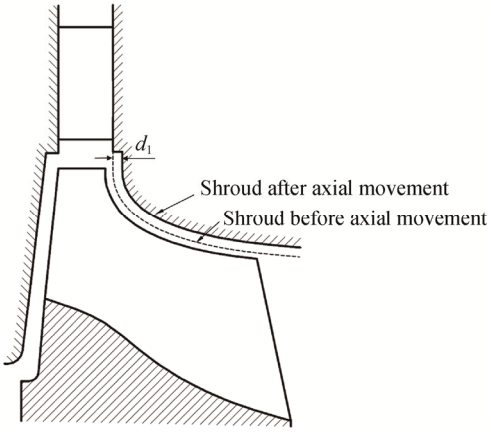


**Fig. 7** Meridional view of the tip clearance changing due to the shroud axial movement

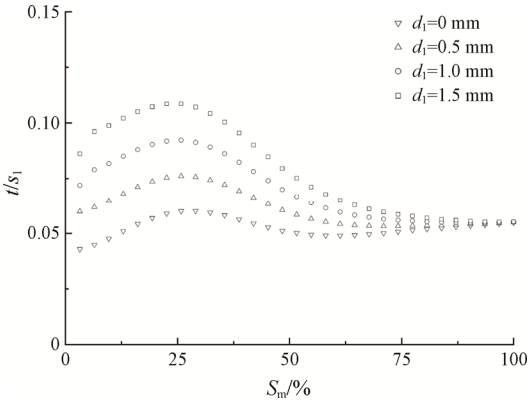


**Fig. 8** Variation of the tip clearance height against Sm for different cases of $d_1$

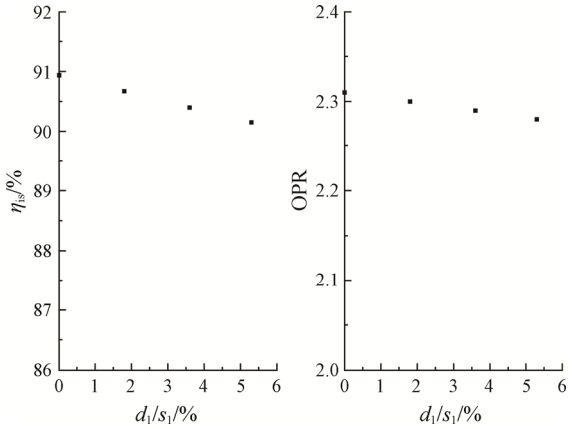


**Fig. 9** Isentropic efficiency and output power against the shroud axial movement $d_1$ for ZK2000S

The shape of the tip clearance vs. $S_m$ curve can also change when the rotor shroud moves radially, as shown in Fig. 10. Fig. 11 shows the isentropic efficiency and output power against the shroud radial movement $d_2$ for ZK2000S turbine. First, as expected, when $d_2$ is increased the exducer radial tip clearance increases and the turbine efficiency decreases. 1% increase of the dimensionless radial clearance $d_2/s_2$ decreases the efficiency by only 0.12%. This is different from that observed by Futral and Holeski [6] who concluded that for each percent increase in radial clearance at the rotor exit, the efficiency is decreased by 1.6%. Second, it is interesting to find that the output power decreases at first, reaches its minimum near $d_2/s_2$=1%, and then increases after the minimum. This is because as $d_2$ increases, the mass flow rate of the turbine increases, as shown in Fig. 12, which benefits the output power of the turbine. This effect offsets the power decrease brought about by the efficiency drop, gradually balancing at first and then exceeding it.

Fig. 13 shows the entropy contours at six streamwise cut planes in the impeller passage. Their locations are shown on the left side of Fig. 13, while the entropy

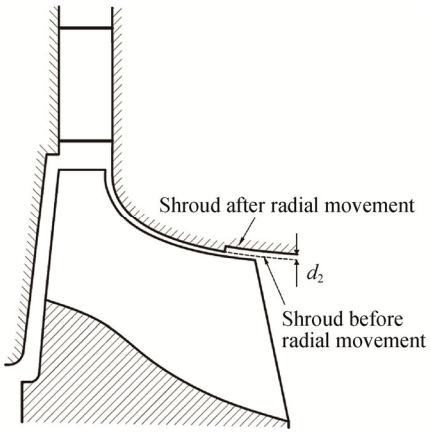


**Fig. 10** Meridional view of the tip clearance changing due to the shroud radial movement

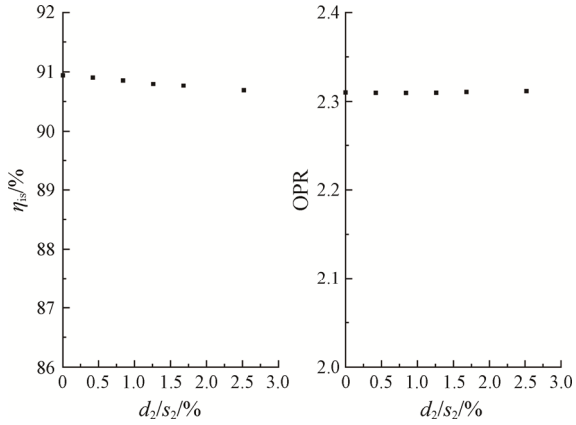


**Fig. 11** Isentropic efficiency and output power vs the shroud radial movement $d_2$ for ZK2000S

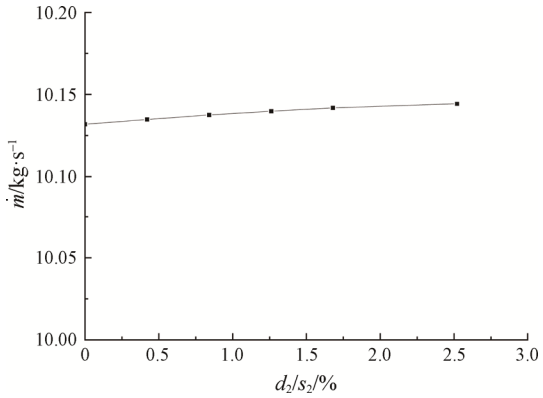


**Fig. 12** Calculated mass flow rate against the shroud radial movement $d_2$ for ZK2000S

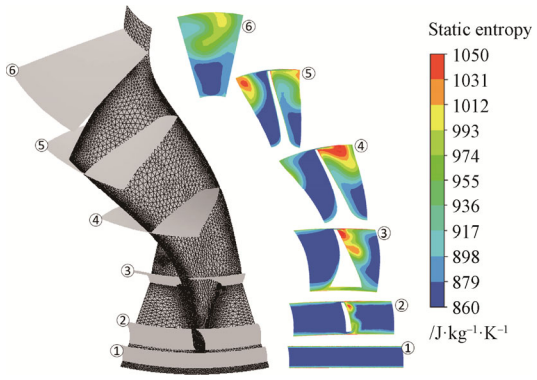


**Fig. 13** Entropy contours at various streamwise cut planes in the impeller passage

contour at each plane for the configuration without shroud deformation is shown on the right side. It shows a general development process of the entropy rise in the impeller passage. In cut plane 1, main stream flow has relatively small entropy, while high entropy regions are near the hub and shroud due to friction. In cut plane 2, entropy starts to rise on the suction surface of the blade, especially near the hub and shroud areas. This is due to the leakage flows from the tip clearance and backface clearance. In cut plane 3, high entropy area is still found on the suction side of the blade, but more concentrates near the shroud which shows that the tip clearance flow has more influence on the turbine performance. With the flow gradually mixed up, the high entropy area gets diffused away and finally dominates the higher parts of the fluid passage, as shown in the cut plane 4 to cut plane 6.

Fig. 14 compares at the cut plane 2 the entropy contour and the tip clearance flow structure between the configuration without shroud deformation and the configuration with a shroud deformation degree of 3°. The results show that the entropy is increased a small amount especially near the shroud region with a stronger leakage flow formed. This is also confirmed by the velocity vector plots, from which we can see that with the shroud deformed to a higher degree, the tip clearance becomes larger and leakage flow stronger. In the suction side of near the blade tip, a vortex is formed due to the scraping effect by the shroud wall. This vortex gets larger due to the increased leakage flow with larger shroud rotation.

Fig. 15 compares at the cut plane 5 the entropy contour and the tip clearance flow structure between the configuration without shroud deformation and the configuration with a shroud deformation degree of 3°. It is obvious that the difference is significant at this

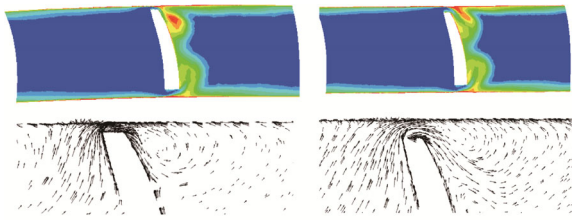

(a) Shroud rotate degree=0° (b) Shroud rotate degree = 3°

**Fig. 14** Comparison of tip clearance flow structure at cut plane 2

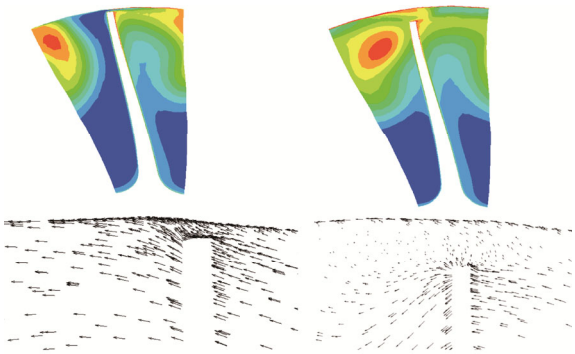

(a) Shroud rotate degree=0° (b) Shroud rotate degree=3°

**Fig. 15** Comparison of tip clearance flow structure at cut plane 5

downstream location of these two configurations. First, the high entropy region almost dominates the entire flow passage near the shroud representing a large flow loss here for the case with shroud deformation. For the case without shroud rotation, flow on the pressure side still shows low entropy. Second, in the velocity vector plots, it can be seen that there is a stronger secondary flow near the shroud area for the case with shroud deformation due to the scraping effect.

### 4.2 Effect of the backface clearance flow

In this section, the effect of backface clearance changing due to rotation of the stationary hub is analyzed, as shown in Fig. 16. The four cases analyzed are with $\theta_h$ values of –2°, ori (no rotation), 1°, and 2°. Their backface clearance heights, $b$, against the Radial Location RL are compared and shown in Fig. 17. The isentropic efficiency and output power against the hub rotating angle are shown in Fig. 18. The results show that as the rotating angle increases and the tip clearance narrows, the efficiency and output power increase. One-degree change of the hub brings about 0.1 percentage of efficiency increase, which is a much smaller influence compared to that of changing the tip clearance.

The shape of the backface clearance can also be changed when the stationary hub moves axially, as shown in Fig. 19. Fig. 20 shows the isentropic efficiency and

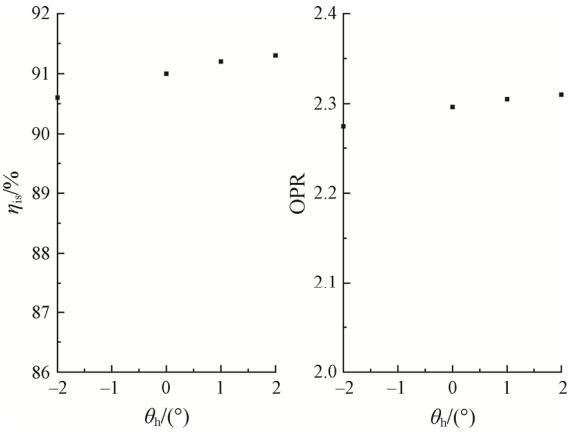


**Fig. 18** Isentropic efficiency and output power against the hub deformation for ZK2000S

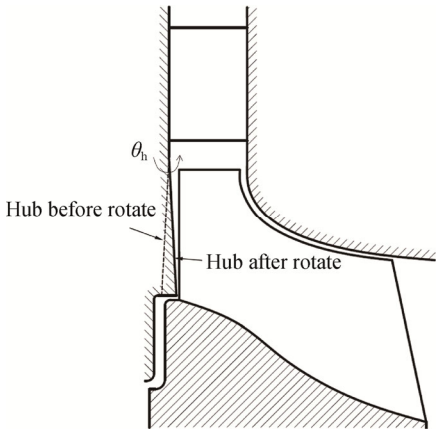


**Fig. 16** Meridional view of the backface clearance changing due to the hub rotating

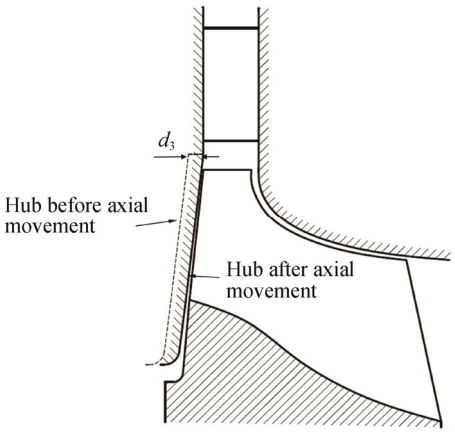


**Fig. 19** Meridional view of the backface clearance changing due to the hub axial movement

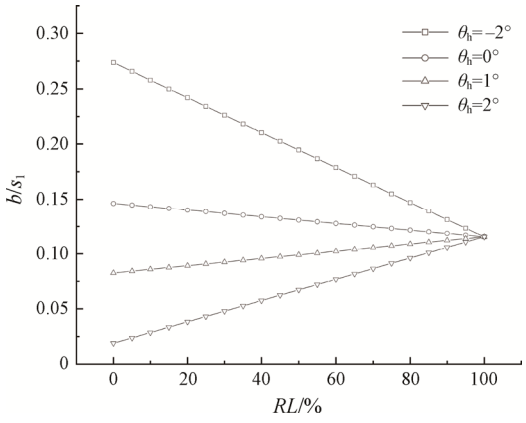


**Fig. 17** Variation of the back clearance height against RL for different $\theta_h$ cases

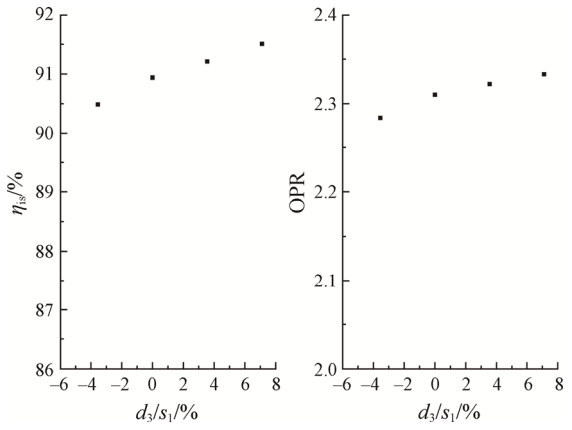


**Fig. 20** Isentropic efficiency and output power against the hub axial movement $d_3$ for ZK2000S

output power compared to the hub axial movement $d_3$. The results show that as $d_3$ increases and the backface clearance becomes smaller, the efficiency and output power increase; however, the influence is much smaller as with changing $\theta_h$. One percentage of $d_3/s_2$ increase only brings about 0.08% of efficiency increase.

Fig. 21 shows the entropy contour and the backface clearance flow structure at the cut plane 2 for hub deformations of –2° and 2°. The results show that the entropy contour and the backface clearance flow structure are similar for the both cases with hub rotatations of –2° and 2°. Entropy is increased on the suction surface of the blade, especially near the hub and shroud areas due to the leakage flows from the tip clearance and backface clearance. The details of the backface clearance flow are shown in the velocity vector plot. Flow is from the pressure side to the suction side and a vortex is formed near the suction side due to the scraping of the hub wall.

Fig. 22 compares at the cut plane 3 the entropy contour and the backface clearance flow structure between the configurations with the hub deformation of –2° and 2°. The results show that there are two regions of high entropy. First, with –2° hub rotation, the tip leakage clearance flow causes high entropy on the suction side near the shroud with a larger area. Second, the backface leakage clearance flow causes high entropy near the hub

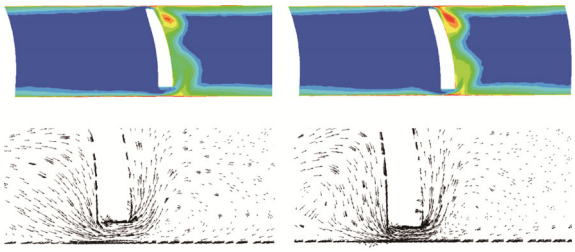

(a) Hub rotate degree=–2° (b) Hub rotate degree=2°

**Fig. 21** Comparison of backface clearance flow structure at cut plane 2

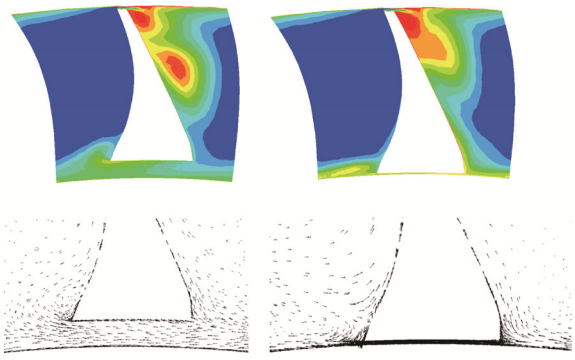

(a) Hub rotate degree=–2° (b) Hub rotate degree=2°

**Fig. 22** Comparison of backface clearance flow structure at cut plane 3

on both the suction and pressure side of the blade. Because of the larger clearance with –2°, the clearance flow is stronger than that with +2° causing a different flow structure. In the case with hub rotation of –2°, a small vortex is formed on the pressure side near the hub. While for the case of 2°, no such vortex is observed.

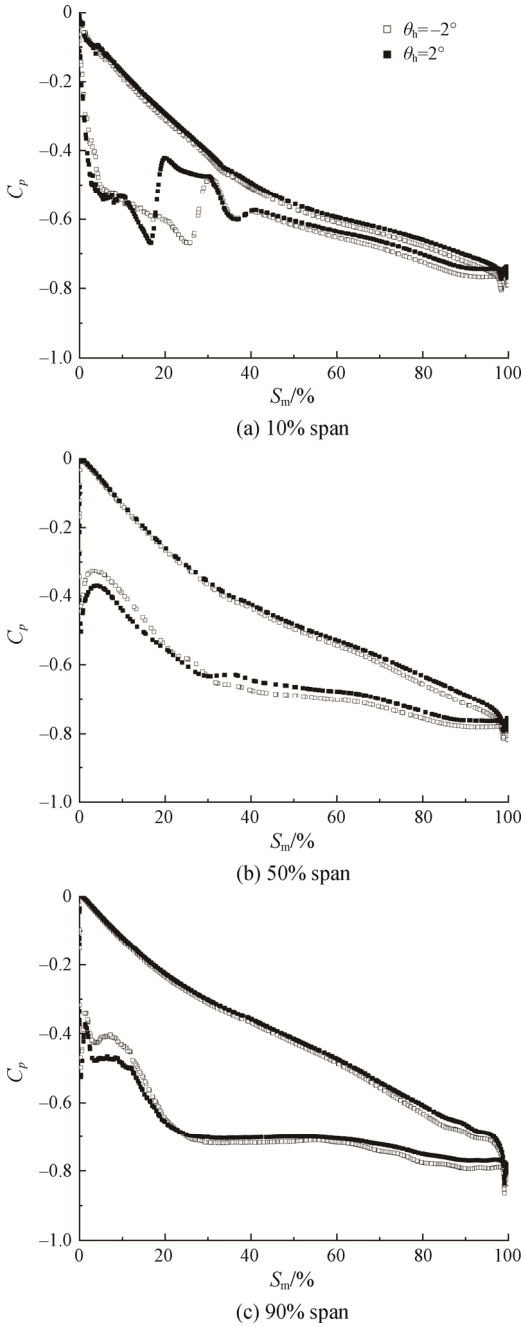


(a) 10% span

(b) 50% span

(c) 90% span

**Fig. 23** Comparison of $C_p$ on rotor pressure and suction surface at different blade span

It is worth noting that at the cut plane 2, which is close to the turbine inlet, the leakage flow due to the pressure difference between the pressure and suction side of the

blade dominates the backface clearance flow. But at the cut plane 3 at smaller radius, it is the scraping flow that dominates the backface clearance flow.

In order to investigate the static pressure distribution on the blade surface, a non-dimensional pressure coefficient $C_p$ is defined:

$$C_p = \frac{p - p_2}{\frac{1}{2}\rho_3 V_3^2} \tag{1}$$

where $p$ is the local static pressure; $p_3$ is the averaged static pressure at the rotor inlet; $\rho_3$ is the averaged density at the rotor inlet, and $V_3$ is the averaged velocity at the rotor inlet.

Fig. 23 shows the $C_p$ distribution on the rotor pressure and suction surface at 10%, 50%, and 90% blade span respectively, and differences are compared between hub rotation angle of –2° and 2°. The hub rotation angle, $\theta_h$, mainly influences the loading distribution at 10% blade span, with little effect at 50% and 90% span. Also, the pressure difference between the pressure and suction surface is reduced significantly at 10% span near the region of the scallop rim. This phenomenon is also well reported by He [5]. Because of this drastic pressure difference reduction, the leakage flow in the backface clearance is weakened and the scraping flow gets stronger. This phenomenon is confirmed with comparing the vector plots at cut plane 2 and 3 in Fig. 21 and 22, respectively. Finally, increasing the hub rotation angle $\theta_h$ from –2° to 2° causes the region of pressure difference reduction to become much larger. Hence, one can expect that more regions of the backface clearance would be dominated by the scraping flow for the case of 2° than for the case of –2°.

## 5. Conclusions

In this paper, influences of various geometry features on the performance of a high-speed radial inflow turbine are investigated. They include: turbine tip and backface clearances; the rounding of exducer trailing edge for natural frequency tuning; and losses due to misalignment of the separate inducer and exducer. Regarding the tip and backface clearances, purely radial and axial motion as well as rotation of the static structures is investigated numerically. Several conclusions are found as follows:

(1) Tip clearance flow plays a more important role affecting the performance of the turbine than the other geometry features studied in this paper. When the tip clearance is enlarged due to the shroud deformation, the reduction of the efficiency is almost linear, and a one degree change of the shroud brings approximately a 1.3% efficiency reduction. When tip clearance is changed by purely axial motion, a 1% increase of the clearance $d_1/s_1$ leads to a 0.15% efficiency reduction. For purely radial increase in exit tip clearance, a 1% increase of the clearance $d_2/s_2$ leads to a 0.12% efficiency reduction. This result is much smaller than that observed by Futral and Holeski [6], who concluded that for each percent increase in rotor exit radial clearance, the efficiency decreases by 1.6%.

(2) The backface clearance flow structure changes for different locations in the flow path. In areas close to the turbine inlet, the leakage flow is primarily a function of the pressure difference between the pressure and suction side of the blade. In areas close to the turbine shaft, it is the scraping motion that dominates the backface clearance flow structure.

(3) The pressure difference between the rotor pressure and suction side surface is reduced significantly at lower blade span near the region of the scallop rim. This conclusion result is consistent with the results from He [5]. Because of this drastic pressure difference reduction, the backface clearance leakage flow is weakened and the scraping flow dominates. Increasing the hub rotation angle $\theta_h$ causes the region of pressure difference reduction to become much larger. Hence, a larger region of the backface clearance would be dominated by the scraping flow rather than the leakage flow.

(4) Nearly 80% of the total output power comes from the inducer, while only 20% is produced by the exducer. Because of this power split, the exducer rounded trailing edge rings has only a small influence on the turbine performance. The turbine with rounded trailing edge has only a 0.12% reduction in efficiency compared with straight trailing edge.

## Acknowledgements

This work was supported by the Key Programs of Chinese Academy of Sciences under Project No. ZDRW-CN-2017-2, Innovation Academy of Light-duty Gas Turbine with Project No. CXYJJ19-ZD-01, and Changde Institute for Integrated Energy Technology with Project No. E164291C01.

## References

[1] Rodgers C., Review of mixed flow and radial turbine options. AIAA Paper, 1990, No. 90-2414.

[2] Jones A.C., Design and test of a small, high pressure ratio radial turbine. ASME Journal of Turbomachinery, 1996, 118(2): 362–370.

[3] Simonyi P.S., Boyle R.J., Comparison of a quasi-3D analysis and experimental performance for three compact radial turbines. AIAA Paper, 1991, No. 91-2128.

[4] He P., Sun Z.G., Chen H.S., Tan C.Q., Investigation of backface cavity sealing flow in deeply scalloped radial

turbines. IMech Part G: Journal of Power and Energy, 2012, 226(6): 751–763.

[5] He P., Chen H.S., Tan C.Q., Aerothermal investigation of backface clearance flow in deeply scalloped radial turbines. Journal of Turbomachinery, 2013, 135: 021002.

[6] Futral S.M., Holeski D.E., Experimental results of varying the blade-shroud clearance in a 6.02-inch radial inflow turbine. NASA 1970, TND-5513.

[7] Dambach R., Hodson H.P., Huntsman I., An experimental study of tip clearance flow in a radial inflow turbine. ASME Journal of Turbomachinery, 1999, 121: 644–650.

[8] Dambach R., Hodson H.P., Tip leakage flow in a radial inflow turbine with varying gap height. AIAA Journal of Propulsion and Power, 2001, 17: 644–650.

[9] Dambach R., Hodson H.P., An experimental study of tip clearance flow in a radial inflow turbine. ASME Turbo Expo, 1998, 98-GT-467.

[10] Deng Q.H., Niu J.F., Feng Z.P., Tip leakage flow in radial inflow rotor of a microturbine with varying blade-shroud clearance. ASME Turbo Expo, 2007, GT2007-27722.

[11] Furukawa M., Inoue, M., Saiki, K., et al., The role of tip leakage vortex breakdown in compressor rotor aerodynamics. ASME Journal of Turbomachinery, 1999, 121: 469–480.

[12] Li W., Wang X., Zhang X.H., et al., Experimental and numerical investigations of closed radial inflow turbine with labyrinth seals. ASME Journal of Engineering for Gas Turbines and Power, 2018, 140: 102502.

[13] Liu H., Romagnoli A., Ricardo M.B., et al., Multi-injection turbine housing: a novel concept for tip-leakage improvement in radial turbines. ASME Turbo Expo, 2017, GT2017-63975.

[14] Huang W.L., Zhao H.J., Wang Z.H., Xi G., Numerical study on interaction of tip synthetic jet with tip leakage flow in centrifugal impeller. ASME Turbo Expo, 2018, GT2018-76330.

[15] Wang N.A., Sun X.J., Huang D.G., Design and analysis of a single-stage transonic centrifugal turbine for Organic Rankine Cycle (ORC). Journal of Thermal Science, 2020, 29(1): 32–42.